Absolute gas density profiling in high-order harmonic generation

Antoine Comby, S. Beaulieu, Eric Constant, D. Descamps, S. Petit, Y. Mairesse

Research Article | Vol. 26, No. 5 | 5 Mar 2018 | OPTICS EXPRESS 6001
Optics EXPRESS

Absolute gas density profiling in high-order harmonic generation

A. Comby,[1,*] S. Beaulieu,[1,2] E. Constant,[3] D. Descamps,[1] S. Petit,[1] and Y. Mairesse[1]

[1] *Université de Bordeaux - CNRS - CEA, CELIA, UMR5107, F33405 Talence, France*
[2] *Institut Natinal de la Recherche Scientifique, Varennes, Quebec, Canada*
[3] *Université Lyon I, CNRS, Laboratoire de Spectrométrie Ionique et Moléculaire, UMR 5579, F69622 Villeurbanne, France*
[*] *antoine.comby@u-bordeaux.fr*

Abstract: We propose and implement a method to determine the absolute density profile of a gas jet producing high-order harmonics. By measuring the transverse profile of the fluorescence emitted by the plasma, we retrieve the local density in the gas jet. We use this technique during the optimization of the high-harmonics of 515 nm, 10 μJ, 130 fs pulses at 500 kHz and find that we can generate in absorption-limited conditions.

OCIS codes: (190.4160) Multiharmonic generation; (190.7110) Ultrafast nonlinear optics; (020.1670) Coherent optical effects; (020.2649) Strong field laser physics.

References and links

1. A. McPherson, G. Gibson, H. Jara, U. Johann, T. S. Luk, I. A. McIntyre, K. Boyer, and C. K. Rhodes, "Studies of multiphoton production of vacuum-ultraviolet radiation in the rare gases," J. Opt. Soc. Am. B **4**, 595–601 (1987).
2. M. Ferray, A. L'Huillier, X. F. Li, L. A. Lompre, G. Mainfray, and C. Manus, "Multiple-harmonic conversion of 1064 nm radiation in rare gases," J. Phys B **21**, L31 (1988).
3. M. Y. Kuchiev, "Atomic antenna," Soviet J. Exper. Theor. Phys. Lett. **45**, 404 (1987).
4. P. B. Corkum, "Plasma perspective on strong field multiphoton ionization," Phys. Rev. Lett. **71**, 1994–1997 (1993).
5. K. J. Schafer, B. Yang, L. F. DiMauro, and K. C. Kulander, "Above threshold ionization beyond the high harmonic cutoff," Phys. Rev. Lett. **70**, 1599–1602 (1993).
6. P. Balcou, P. Salières, A. L'Huillier, and M. Lewenstein, "Generalized phase-matching conditions for high harmonics: The role of field-gradient forces," Phys. Rev. A **55**, 3204–3210 (1997).
7. E. Constant, D. Garzella, P. Breger, E. Mével, C. Dorrer, C. Le Blanc, F. Salin, and P. Agostini, "Optimizing High Harmonic Generation in Absorbing Gases: Model and Experiment," Phys. Rev. Lett. **82**, 1668–1671 (1999).
8. J. Boullet, Y. Zaouter, J. Limpert, S. Petit, Y. Mairesse, B. Fabre, J. Higuet, E. Mével, E. Constant and E. Cormier, "High-order harmonic generation at a megahertz-level repetition rate directly driven by an ytterbium-doped-fiber chirped-pulse amplification system," Opt. Lett. **34**, 1489 (2009).
9. J. Rothhardt, M. Krebs, S. Hädrich, S. Demmler, J. Limpert, and A. Tünnermann, "Absorption-limited and phase-matched high harmonic generation in the tight focusing regime," New J. Phys. **16**, 033022 (2014).
10. C. M. Heyl, H. Coudert-Alteirac, M. Miranda, M. Louisy, K. Kovacs, V. Tosa, E. Balogh, K. Varjú, A. L'Huillier, A. Couairon, and C. L. Arnold, "Scale-invariant nonlinear optics in gases," Optica **3**, 75 (2016).
11. A. Cabasse, G. Machinet, A. Dubrouil, E. Cormier, and E. Constant, "Optimization and phase matching of fiber-laser-driven high-order harmonic generation at high repetition rate," Opt. Lett. **37**, 4618–4620 (2012).
12. A. Cabasse, C. Hazera, L. Quintard, E. Cormier, S. Petit, and E. Constant, "Collection and spectral control of high-order harmonics generated with a 50 W high-repetition rate Ytterbium femtosecond laser system," J. Phys. B: At. Mol. Opt. Phys. **49**, 085601 (2016).
13. Lorek, E., Larsen, E. W., Heyl, C. M., Carlström, S., Paleček, D., Zigmantas, D., and Mauritsson, J. " High-order harmonic generation using a high-repetition-rate turnkey laser," Rev. Sci. Instrum. **85**(12), 123106 (2014).
14. C. M. Heyl, C. L. Arnold, A. Couairon, and A. L'Huillier, "Introduction to macroscopic power scaling principles for high-order harmonic generation," J. Phys. B **50**, 013001 (2017).
15. S. Hädrich, M. Krebs, A. Hoffmann, A. Klenke, J. Rothhardt, J. Limpert, and A. Tünnermann, "Exploring new avenues in high repetition rate table-top coherent extreme ultraviolet sources," Light Science Appl. **4**, e320 (2015).
16. S. Hädrich, Jan Rothhardt, M. Krebs, S. Demmler, A. Klenke, A. Tünnermann, and J. Limpert, "Single-pass high harmonic generation at high repetition rate and photon flux," J. Phys. B **49**, 172002 (2016).
17. R. Klas, S. Demmler, M. Tschernajew, S. Hädrich, Y. Shamir, A. Tünnermann, J. Rothhardt, and J. Limpert, "Table-Top Milliwatt-Class Extreme Ultraviolet High Harmonic Light Source," Optica **3**, 1167, (2016)

#319616 https://doi.org/10.1364/OE.26.006001
Journal © 2018 Received 12 Jan 2018; revised 14 Feb 2018; accepted 14 Feb 2018; published 27 Feb 2018

Optics EXPRESS

18. C. Altucci, C. Beneduce, R. Bruzzese, C. d. Lisio, G. S. Sorrentino, T. Starczewski, and F. Vigilante, "Characterization of pulsed gas sources for intense laser field - atom interaction experiments," J. Phys. D Appl. Phys. **29**, 68–75 (1996).
19. A. Behjat, G. J. Tallents, and D. Neely, "The characterization of a high-density gas jet," J. Phys. D Appl. Phys. **30**, 2872 (1997).
20. V. Malka, , C. Coulaud, , J. P. Geindre, , and, V. Lopez, Z. Najmudin, D. Neely, and F. Amiranoff, "Characterization of neutral density profile in a wide range of pressure of cylindrical pulsed gas jets," Rev. Sci. Instrum. **71**, 2329–2333 (2000).
21. F. Brandi and F. Giammanco, "Temporal and spatial characterization of a pulsed gas jet by a compact high-speed high-sensitivity second-harmonic interferometer," Opt. Express **19**, 25479–25487 (2011).
22. B. H. Failor, S. Chantrenne, P. L. Coleman, J. S. Levine, Y. Song, and H. M. Sze, "Proof-of-principle laser-induced fluorescence measurements of gas distributions from supersonic nozzles," Rev. Sci. Instrum. **74**, 1070–1076 (2003).
23. P. W. Wachulak, . Węgrzyński, Z. Zápražný, A. Bartnik, T. Fok, R. Jarocki, J. Kostecki, M. Szczurek, D. KorytÃąr, and H. Fiedorowicz, "Extreme ultraviolet tomography of multi-jet gas puff target for high-order harmonic generation," Appl. Phys. B **117**, 253–263 (2014).
24. N. E. Schofield, D. M. Paganin, and A. I. Bishop, "Absolute density-profile tomography of molecular beams using multiphoton ionization," Rev. Sci. Instrum. **80**, 123105 (2009).
25. O. Tchulov, M. Negro, S. Stagira, M. Devetta, C. Vozzi, and E. Frumker, "Laser induced strong-field ionization gas jet tomography," Sci. Rep. **7**, 6905 (2017)
26. M. J. Thorpe, F. Adler, K. C. Cossel, M. H. de Miranda, and J. Ye, "Tomography of a supersonically cooled molecular jet using cavity-enhanced direct frequency comb spectroscopy," Chem. Phys. Lett. **468**, 1–8 (2009).
27. L. Lavenu, M. Natile, F. Guichard, Y. Zaouter, M. Hanna, E. Mottay, and P. Georges, "High-energy few-cycle Yb-doped fiber amplifier source based on a single nonlinear compression stage," Opt. Express **25**, 7530 (2017).
28. S. Beaulieu,E. Bloch, L. Barreau,A. Comby,D. Descamps,R. Géneaux,F. Légaré,S. Petit, and Y. Mairesse, "Phase-resolved two-dimensional spectroscopy of electronic wave packets by laser-induced XUV free induction decay" Phys. Rev. A **95**, 041401 (2017).
29. S. Kazamias, S. Daboussi, O. Guilbaud, K. Cassou, D. Ros, B. Cros, and G. Maynard, "Pressure-induced phase matching in high-order harmonic generation," Phys. Rev. A **83**, 063405 (2011).
30. E. Priori, G. Cerullo, M. Nisoli, S. Stagira, S. De Silvestri, P. Villoresi, L. Poletto, P. Ceccherini, C. Altucci, R. Bruzzese, and others, "Nonadiabatic three-dimensional model of high-order harmonic generation in the few-optical-cycle regime," Phys. Rev. A **61**, 063801 (2000).
31. B. Henke, E. Gullikson, and J. Davis, "X-ray interactions: Photoabsorption, scattering, transmission, and reflection at e = 50-30,000 ev, z = 1-92," Atomic Data Nucl. Data Tab. **54**, 181 – 342 (1993).
32. A. Paul, E. Gibson, X. Zhang, A. Lytle, T. Popmintchev, X. Zhou, M. Murnane, I. Christov, and H. Kapteyn, "Phase-Matching Techniques for Coherent Soft X-Ray Generation," IEEE J. Quantum Electron. **42**, 14–26 (2006).

1. Introduction

The thickness of non-linear crystals is a crucial parameter in optical harmonic generation. It determines the conversion efficiency, through a trade-off between the increase of generation volume and the phase matching conditions. High-order harmonic generation (HHG) is an extremely non-linear process, in which the non-linear medium is generally a gas [1, 2]. HHG occurs when atoms or molecules interact with an intense laser pulse (few 10^{13} – 10^{14} W/cm^2). On the microscopic scale, the laser field ionizes the atom/molecule, accelerates the freed electrons and drives them back to recombine with their parent ion, resulting in the emission of extreme ultraviolet (XUV) radiation [3–5]. On the macroscopic scale, the build-up of the XUV emission is efficient only if the atomic emitters radiate in phase [6, 7]. This phase-matching constraint, which is conceptually similar to the one encountered in non-linear optical crystals, has few specificities.

Phase-matching in HHG is achieved when the generated XUV remains in phase with the fundamental field throughout the generating medium. The first factor that influences this phase matching is the medium dispersion between the visible and XUV. Two terms actually play a role: the dispersion by the neutral gas and by the ionized electrons. Both are proportional to the medium density and length, and the latter strongly depends on the laser intensity. The second important factor for phase matching is related to the geometry of the interaction where the spatial phase associated to the focusing of the fundamental laser, known as the Gouy phase, becomes particularly important in the tight focusing configuration. The last contribution to phase matching is the so-called atomic dipole phase, which is intrinsic to the HHG mechanism and depends on the laser intensity and the spatial profile.

Optics EXPRESS

In the low ionization regime, under a critical ionization rate, phase matching is achieved by tuning the gas density in such way that the positive dispersion phase mismatch compensates the negative geometrical and atomic dipole phase mismatches. Under these conditions, the XUV emission scales as the squared number of emitters, i.e. as the squared density. However as the density increases, the reabsorption of the generated harmonics by the medium starts to play a role and limits the output XUV flux. The optimal generating conditions, balancing coherence and absorption, are typically reached when the coherence length l_{coh}, the absorption length l_{abs} and the medium length l_{med} fulfill $l_{coh} > 5l_{abs}$ and $l_{med} > 3l_{abs}$ [7]. Since all these parameters are influenced by the medium density and length, it becomes essential to control and monitor them precisely.

This need becomes even more critical when HHG is performed with high repetition rate lasers [8]. For instance, fiber lasers have great advantages in terms of flux, stability and spatial mode, but their low energy per pulse (few tens of μJ) imposes a tight focusing to reach the $\sim 10^{13} - 10^{14}$ W/cm^2 intensity range. This tight focusing configuration increases the geometrical phase mismatch, considerably reducing the coherence length. Recent investigations [9, 10] have demonstrated that efficient HHG could nevertheless still be achieved if the generating medium parameters (length, density, ...) were properly scaled. If the waist at the focus is reduced by a scaling factor s by increasing the numerical aperture NA = w_1/f (w_1 is the beam waist before focusing and f the focal length), the medium length should be shorten by s^{-2} and the density increased by s^2 in order to keep the same HHG efficiency.

With these considerations, several works reported on the generation of XUV light with a high conversion efficiency when driving HHG using μJ-level pulses [9–17]. The quadratic dependence of the medium length and density on the scaling factor underlines the sensitivity of the HHG yield to these parameters. Various techniques have been developed to measure the length and the density of a gas jet: interferometric measurements using a Mach-Zender interferometer [18–21], fluorescence [22], XUV absorption [23], ionization measurements [24, 25] and frequency-comb spectroscopy [26]. Most of these techniques require important additional and costly equipment to measure the proprieties of the jet : additional laser beams, XUV radiation or charged-particle spectrometers. Furthermore the most common technique – interferometry – is not very precise for thin gas jets where the phase shifts are induced only on a short length and need high density to be measurable. These methods are thus in practice not implemented in parallel to HHG experiments. The fast growing of reliable, cost effective and flexible high repetition rate Yb:based laser drivers paves the road to high flux stable and agile HHG secondary sources requiring a simple and accurate device to determine routinely the best condition of generation for some given optical parameter. Therefore, we present in this paper a simple technique to characterize both the density and the medium length for optimal and reproducible high harmonic generation.

2. Experimental setup

The experimental setup is described in Fig. 1. We used the BlastBeat femtosecond laser system at CELIA, which consists of a two synchronized 50 W Yb-doped fiber lasers (Tangerine, Amplitude Systemes [27]) delivering 130 fs pulses centered at 1030 nm, at a repetition rate which can be continously tuned between 166 kHz and 2 MHz. For this study we used a single arm, set at 20 W average power and 500 kHz repetition rate. The laser pulses were frequency doubled in a 1 mm thick type I BBO crystal, producing a 5 W at 515 nm with 10 μJ per pulse. The beam was expanded by a $\times$ 2.66 telescope and focused with a f =25 cm lens in an argon gas jet inside a vacuum chamber. The FWHM of the focal spot was measured to be 11 μm with a CCD camera, with a Rayleigh length of 0.75 mm. The pulse energy was measured with a power meter, and the pulse duration was estimated from the duration measurement of the 1030 nm beam (130 fs). The frequency doubling in the 1 mm BBO shortens the 130 fs pulse only by 10-15%. These elements lead us to an estimate intensity of $\sim 4 \times 10^{13}$ W/cm^2, high enough to create a plasma and to

Optics EXPRESS

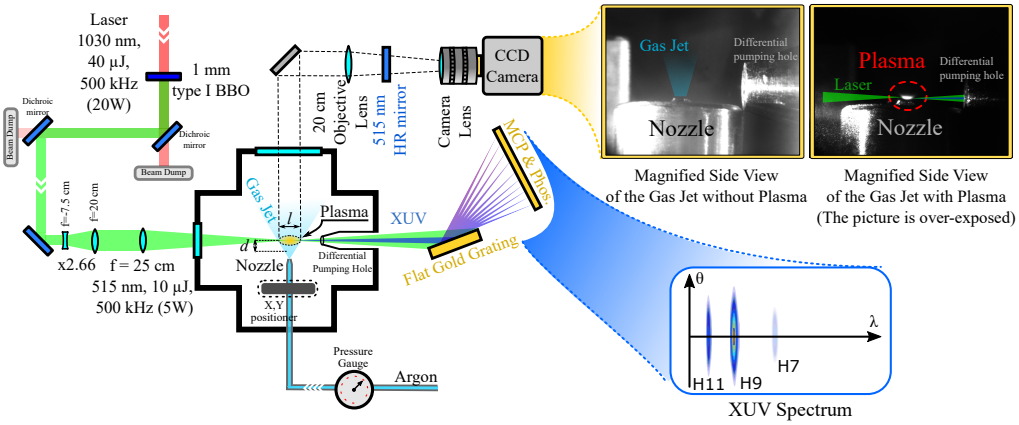

Fig. 1. Scheme of the experimental setup. The 130fs - 40 μJ - 500 kHz pulses @ 1030 nm are sent into a 1 mm thick BBO crystal to provide 10 μJ - 500 kHz pulses at 515 nm. The green beam is expanded in a 2.66 $\times$ telescope and focused by a 25 cm lens into a vacuum chamber, where it interacts with a gas jet. The laser is intense enough to create a plasma and generate HHG. The fluorescence of the plasma is imaged with a 20 cm magnifying lens and a set of camera lenses onto a CCD sensor. In the actual experimental setup, the nozzle is vertical and the imaging system is set on a horizontal plane, orthogonal to the gas jet direction. This imaging allows us to measure the distance d from the nozzle, the length l (FWHM) and the brightness B of the plasma. The HHG spectrum is measured simultaneously by a flat field XUV spectrometer.

generate high order harmonics. The gas jet was produced by a 250 μm nozzle supplied by Ar with a controlled backing pressure between 0.5 and 8 bars. A maximum residual pressure of few 10^{-1} mbar was insured in the generating chamber by a double stage roots-primary pump ADS 602P (Adixen) with a pumping speed of 600 m^3/h. In order to prevent reabsorption, a differential pumping tube was placed close to the laser focus, connecting the generating chamber to a second vacuum chamber pumped by a turbomolecular pump, with a maximum residual pressure of 5 $\times$ 10^{-6} mbar. The XUV radiation was analyzed by a flat field XUV spectrometer, consisting of a 1200 grooves/mm holographic cylindrical grating with variable groove spacing (Shimadzu) and a set of dual micro-channel plates coupled to a P46 phosphor screen (Hamamatsu). A 12-bit cooled CCD camera (PCO) recorded the spatially-resolved harmonic spectrum. The fundamental laser beam was rejected out of the spectrometer by a dielectric D-shaped mirror.

The interaction between the laser and the gas jet creates a shining plasma. This fluorescence was collected by a f =20 cm, 1 inch lens and imaged through camera lenses on an 8-bit CCD camera with a mounted adaptive lens. The two lenses act as a far-field microscope. A high reflecty 515 nm dielectric 0° mirror was used to eject light at the fundamental laser wavelength.

This simple imaging system allows us to measure three parameters :
a) The distance d between the nozzle and the focus of the laser, thanks to our imaging geometry,
b) The length (FWHM) of the plasma l, extracted from a fit of its longitudinal profile,
c) The brightness of the plasma B, defined as the peak intensity of the plasma image.

As explained below, we will use these parameters to measure the absolute density profile of the gas jet.

Optics EXPRESS

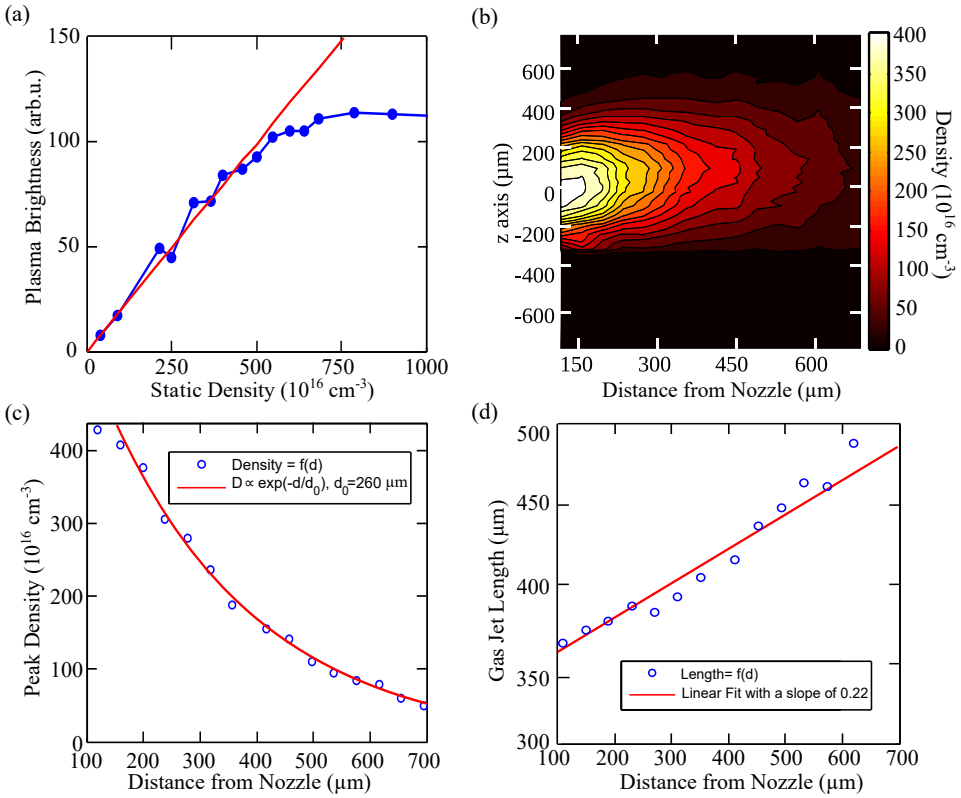

Fig. 2. (a) Plasma brightness as a function of the static Ar density in the closed vacuum chamber. Experimental points (blue) and linear fit (red). (b) Absolute density map of the gas jet produced by a 250 μm nozzle backed with 2 bars of Ar. (c) Peak pressure at different distance of the gas jet, with an exponential decay fit with a characteristic length of 260 μm. (d) Width of the density profile at different distance of the gas jet, with a linear fit with a slope of 0.22 .

3. Absolute density profile of the gas jet

The brightness B of the plasma depends on the laser intensity as well as on the gas density distribution. In order to extract the latter, we used a calibration procedure. We kept the same laser parameters, stopped the pumping by closing the chamber with vacuum valves, and filled in the generating chamber with a static density of argon. The static density of argon was measured with a membrane gauge giving the absolute pressure in the 1-1000 mbar range i.e. in the $\sim$ 2.5-2500 10^{16} cm^{-3} range. We measured the plasma brightness as a function of the argon density (Fig. 2(a)). The brightness increases linearly as the density increases until 500 10^{16} cm^{-3}. This means that B can be used as a direct measurement of the local density in this range.

As the density further increases, the brightness saturates. At 500 10^{16} cm^{-3}, the typical collision time for a excited state of Ar at 300 K is about 5 ns, which is also the typical fluorescence time. The limitation of the linearity around 500 10^{16} cm^{-3} is thus due to the lifetime shortening of the radiative excited Ar states caused by inelastic collision, already observed for XUV emission from Rydberg states [28].

To retrieve the length of a gas jet from the plasma profile, it is necessary to disentangle the contribution from the longitudinal laser intensity profile and from the density profile of the gas jet. To do so, we calibrate the laser contribution by measuring the length of the plasma created

Optics EXPRESS

with the constant gas distribution, i.e. with the vacuum chamber filled by a static argon density. We obtain a gaussian profile with a 1.0 mm FWHM length. All the plasma profiles measured in the gas jet will be divided by this reference distribution to calibrate out the influence of the laser intensity variation and retrieve the gas jet profile. Note that since our gas jet is much shorter than the Rayleigh length, this correction only has a weak influence.

Next we pump down the chamber and back the jet with 2 bars of argon. The plasma fluorescence is imaged for different distances between the nozzle and the laser, from 120 μm to 700 μm by 15 steps. Note that this distance is accurately determined from the images and can be precisely tuned by moving the nozzle with a picomotor. At each distance from the nozzle d, we measure the plasma transverse profile, from which we extract the gas jet length l and the brightness B. We convert B to local density using the calibration of Fig. 2(a), to obtain the density profile of the gas jet shown in Fig. 2(b). The density decreases exponentially with the distance d with a typical length in 1/e of 260 μm as shown in Fig. 2(c). The transverse profile is typically a gaussian with a width (FWHM) that increases also linearly with the distance d. The gaussian profile of the atomic density at a fixed d and the exponential decay of the peak density are typical of effusive gas jets [18, 19]. However, the slow linear growth of the transverse profile is different from a standard model with a freely expanding, low-viscosity fluid for a spatially constant temperature gas, where the transverse profile is independent of d [19]. This means that we are in an intermediate regime between an effusive and a supersonic expansion.

Our measurement technique is conceptually close to the fluorescence technique reported in [22] but it uses the same laser to generate harmonics and to retrieve the density profile, and thus allows to measure the gas jet length and density in real time during HHG experiments. One main advantage of our method is that the signal is quite simple to measure. It is a all-optical technique in the visible range without needing interferometric stability or special image treatment. It is also shown to be very precise for low density gas jet, which can be problematic with standard interferometric measurements. On the other hand, our method has an issue to measure directly high gas density because the brightness saturates at 500 10^{16} cm^{-3}. However, this limitation was not problematic for our study as we get our main results under this limit.It would be still possible to measure indirectly higher density by extrapolating the measurements at lower backing pressure scaled linearly with the backing pressure (the linearity between the local density and the backing pressure was observed in previous studies [18, 20])

4. High order harmonic in a fully characterized gas jet

To enlighten the full potential of this technique, we carried out a study of the high-order harmonic emission while monitoring the density and length of the generating medium. Our typical spectrum is made of the harmonics 7, 9 and 11 of the 515 nm, mainly dominated by H9 with a contrast of 1 : 12 : 2. The evolution of the harmonic flux as a function of the medium peak density is shown in Fig. 3(a). We recorded five sets of measurements at different distances from the nozzle exit, from 120 to 600 μm, and measured medium lengths from 330 to 470 μm. For each scan we varied the backing pressure from 0.5 to 8 bar, and extracted the gas jet density from the plasma brightness calibration. The photon flux was obtained with a calibrated XUV photodiode protected by a 156 nm Al filter. The background signal in the absence of generating gas was checked to be zero, indicating that the fundamental radiation was properly blocked by the filter. The XUV transmission of the Al filter was measured and taken into account to retrieve the photon flux of harmonic available for XUV experiments.

For every distance d from the nozzle, we first observe a fast growth of the high-order harmonic signal with gas density before reaching a saturation followed by a decay. As the medium length increases, the maximum of the HHG signal is reached for lower densities.

According to the analytical formula of [7], the saturation and decay of the HHG flux can have two origins : destructive interferences between the different emitters in the gas or a strong

Optics EXPRESS

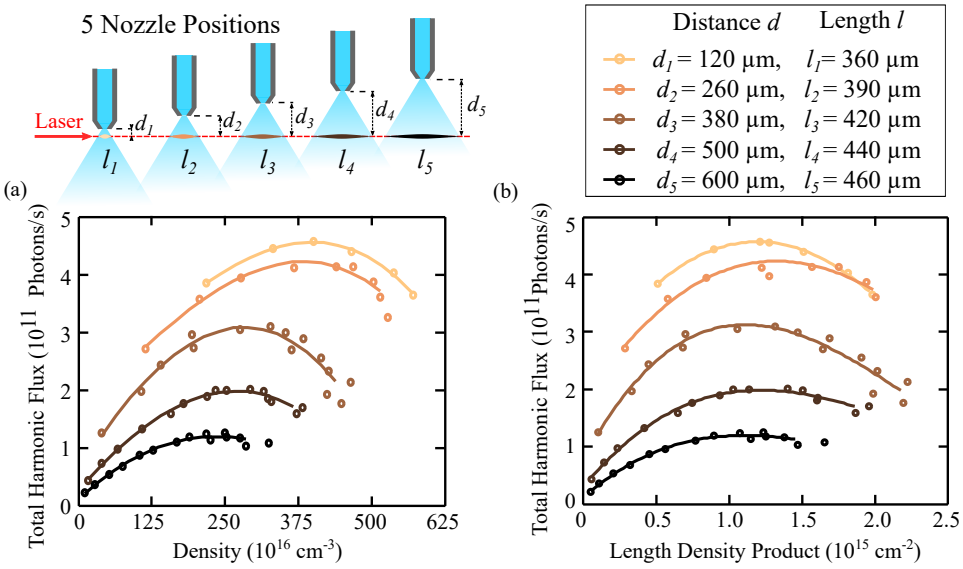

Fig. 3. (a) Harmonic flux as a function of density at different distances from the nozzle. (b) Harmonic flux as a function of length-density product. Circles are the measurements points and the lines a spline smoothing as a guide to the eyes.

reabsorption. Additional processes, not taken into account in the formula, may also play a role, for instance laser defocusing due to the increase of the electron density leading to a transient phase matching which requires numerical model [29, 30]. We will show that our measurement technique enables assigning the decay of the harmonic signal to XUV reabsorption.

The plasma imaging provides the medium length for each point of Fig.3(a). It is then possible to plot the harmonic flux as a function of the length-density product (Fig. 3(b)). The results show that all the curves reach their maxima at the same length-density product of 1.2 10^{15} cm^{-2}. The length-density product is intrinsically related to the quantity of emitters N in the volume. Assuming a cylindrical volume of emission, $N = V \cdot d = S \cdot l \cdot D$, with V the volume of the emitters, S the surface dependent on the waist and intensity of the laser, l the length of the medium and D the atom density. The fact that we observe a maximum signal for a fixed length-density product means that there is a total number of emitters that optimizes the signal, independently of the medium length. We are sure that we are not limited by the longitudinal variation of the intensity along the medium as our confocal parameters (1.5 mm) is much higher than the medium length.

The measurement of the absolute density profile enables the quantitative analysis of the generating conditions through the determination of the three important quantities characterizing the process: the coherence length, the absorption length, and the medium length (equations for the calculation of the coherence length could be find in [9] for instance). The phase mismatch associated to the dispersion of the neutral gas can be calculated using the medium density profile, and refraction indexes from the CXRO database [31]. Since maximum laser intensity of $\sim 4 \times 10^{13}$ W/cm^2 is used in our experiment, dispersion from electron density can be neglected (weak ionization of Ar estimated at 4 10^{-6} from ADK calculation far from the critical ionization fraction at of 5 % [32]). The atomic dipole phase in HHG also plays a negligible role since only short trajectories contribute here in the high-order harmonic signal, as indicated by the narrow spatial and spectral profile of the harmonics. The phase mismatch induced by the geometric focusing of the driving beam (Gouy phase shift) is calculated from the measured beam waist and Rayleigh

Optics EXPRESS

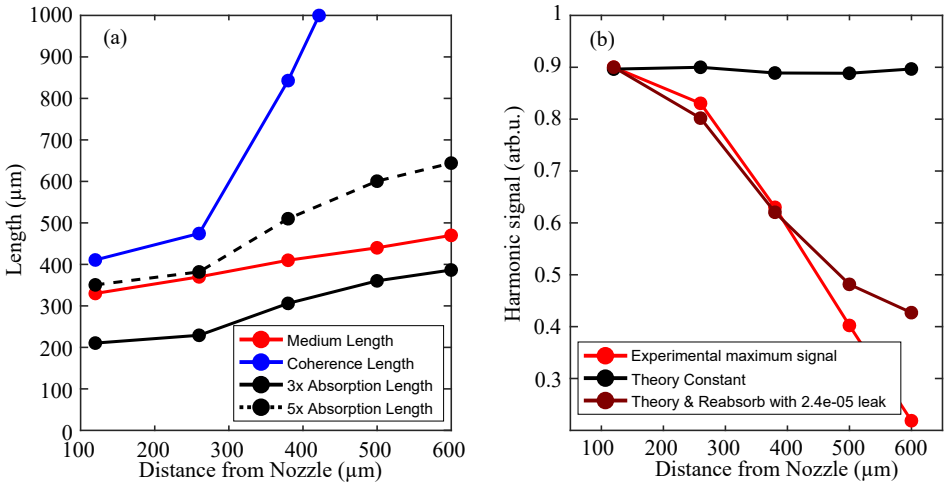

Fig. 4. (a) Medium length, coherence length and absorption length measured at the optimum harmonic signal for each distance from the nozzle. (b) Evolution of the experimental and theoretical optimum harmonic signal as a function of distance.

lengths. Finally, the XUV absorption length is deducted from the atom density measurement, with an absorption cross section that is 3.6×10^{-15} cm^2 for 57 nm wavelength (H9 of 515 nm). Figure 4(a) shows the HHG characteristic lengths as a function of the distance from nozzle. The double conditions for optimization of HHG is fulfilled: $l_{coh} > 5l_{abs}$ and $l_{med} > 3l_{abs}$. We also confirm that the coherence length is always higher than the medium length. Note that the condition $l_{med} > 3l_{abs}$ is equivalent to $l_{med} \cdot \rho \cdot \sigma > 3$ which relate explicitly the density-length product to the cross-section. From our density length of 1.2×10^{15} cm^2 maximizing the signal, we have $l_{med} \cdot \rho \cdot \sigma = 4.3$. This emphasizes that one needs to find the good length product depending on the cross-section.

Even if the harmonic signal always maximizes at the same length-density product, our experiment shows that the maximum signal decreases when the laser is far from the nozzle (Fig. 3(b)). The evolution of the maximum signal as a function of the distance to nozzle is presented in Fig. 4(b), together with the theoretical curve estimated from the formula in [7]. While the theoretical signal remains constant as soon as the double condition is satisfied, the experimental flux clearly decays. We attribute this decay to argon reabsorption effects in the vacuum chamber. As the distance d between the laser focus and the nozzle is increased, the medium is longer but the density decreases exponentially. In order to reach the appropriate length-density product, a higher backing pressure is required, increasing the residual pressure in the HHG pressure up to 0.3 mbar. Even if we placed a differential pumping hole close to the interaction chamber, there seems to be a significant reabsorption of the XUV. Indeed, the experimental data can be nicely reproduced by correcting the theoretical curve by an absorption in $\exp(-\sigma \cdot \eta_{\text{leak}} \cdot P_{\text{back}} \cdot l_{\text{leak}})$, where η_{leak}=2.4 $\times 10^{-5}$ is a leak fraction from the backing pressure P_{back} which absorbs the harmonics over a distance of $l_{\text{leak}} \sim 10$ cm. The leak fraction used for this calculation is consistent with the dimensions of the differential pumping hole and the pumping capacities of our setup.

Our results prove that we can perfectly phase-match the HHG process for a given single-atom response. Our conversion efficiency reaches the 10^{-7} level in argon and is only limited by the atomic dipole response as we worked at quit low intensity. To improve the single-atom response, an higher intensity would be needed, which would lead to higher ionization conditions. In this case, our method would still work as long as there is no strong defocusing, which should be the case in good phase-matching conditions. Note that in strong ionization conditions, the phase-matching

Optics EXPRESS

process becomes a transient process, which evolves on a femtosecond timescale [29]. In that case our method would only determine an average coherence length, but to the best of our knowledge there is currently no other method available to achieve this.

5. Conclusion

We have developed a method allowing to map the absolute density profile of a gas jet, especially well suited for high-order harmonic generation. This technique works even for low density gas targets and is useful to gain deeper insight in HHG and to maximize the XUV photons flux. We have applied the method to HHG by low energy femtosecond pulses in a tight focusing configuration, and showed that it provides a way to determine the medium and coherence lengths and to identify the limitation of our setup by reabsorption effects. When reabsorption effects are low, i.e. when the nozzle is close to the laser focus, we obtain a conversion efficiency of 10^{-7} for the HHG process. This efficiency is limited by the intensity of the laser pulses, and could be improved by increasing the laser power to work with higher energy pulses. The great advantages of the technique presented here are its accuracy, its easy installation and calibration, and the possibility to use it simultaneously with the high harmonic generation, allowing to optimize the XUV flux in a controlled and reproducible manner.

Funding

NSERC Vanier Scholarship. European Research Council (ERC 682978 - EXCITERS); French National Research Agency through (ANR-14-CE32-0014 MISFITS).

Acknowledgments

The authors thank R. Bouillaud, L. Merzeau, N. Fedorov for technical support and T. Ruchon for fruitful discussion.